Effects of Thermal Treatment and Fluoride Ion doping on surface and Catalytic properties of NiO-ZrO2 catalysts.

Abstract:

Abstract. ZrO2 and a series of NiO/ZrO2 hydrogels (5-25 wt% NiO) were co-precipitated with the aid of NaOH-Na2C2O4 solution. Two fluorinated hydrogels were also prepared by wet impregnation method. The samples were calcined in the temperature range 550-850oC. The surface properties of the samples were determined using DTA, XRD and nitrogen adsorption at 77 K. The conversion of isopropanol was tested using microcatalytic pulse technique. DTA measurements showed that the addition of nickel oxide to zirconia influences the phase transition of ZrO2. XRD reveals that the tetragonal phase was formed at ≤ 650oC while a biphasic mixture was obtained at ≥ 750oC. No spinel structure was detected by both DTA and XRD techniques and only traces of cubic NiO were detected for samples containing ≥ 15 wt% nickel oxide and calcined at ≥ 750oC. Significant changes in texture, surface acidity and catalytic activity were found as a result of the effects of thermal treatment and chemical composition. Incorporation of fluoride ion greatly increased the surface acidity and consequently enhanced the dehydration activity. Dehydration activity is related to the amount of surface acidity while the dehydrogenation of this alcohol is sensitive to NiO content.

Authors:

Reham Mohamed Abdel Fattah	faculty of Sciences ,Damietta university
Dr HALA AHMED KIWAAN	Chemistry Department, Faculty of Science, Damietta University, Damietta, Egypt, 34517.
Prof. AWAD IBRAHEEM AHMED	Chemistry Department, Faculty of Science, Mansoura University, Mansoura, Egypt,35516.
Prof. MOHAMED RAMZY MOSTAFA	Chemistry Department, Faculty of Science, Damietta University, Damietta, Egypt, 34517.

Keywords:

NiO supported Zirconia, acidity of solid catalyst, isopropanol conversion

Effects of Thermal Treatment and Fluoride Ion Doping on Surface and Catalytic Properties of NiO-ZrO_2 Catalysts.

REHAM M. ABDEL FATTAH [1,*], HALA A. KIWAN [1], AWAD I. AHMED [2], MOHAMED R. MOSTAFA [1].

[1]Chemistry Department, Faculty of Science, Damietta University, Damietta, 34517, Egypt.

[2]Chemistry Department, Faculty of Science, Mansoura University, Mansoura, 35511, Egypt.

E-mail: rehamfattah2012@gmail.com

Abstract. ZrO_2 and a series of NiO/ZrO_2 hydrogels (5-25 wt% NiO) were co-precipitated with the aid of NaOH-$Na_2C_2O_4$ solution. Two fluorinated hydrogels were also prepared by wet impregnation method. The samples were calcined in the temperature range 550-850°C. The surface properties of the samples were determined using DTA, XRD and nitrogen adsorption at 77 K. The conversion of isopropanol was tested using microcatalytic pulse technique. DTA measurements showed that the addition of nickel oxide to zirconia influences the phase transition of ZrO_2. XRD reveals that the tetragonal phase was formed at ≤ 650°C while a biphasic mixture was obtained at ≥ 750°C. No spinel structure was detected by both DTA and XRD techniques and only traces of cubic NiO were detected for samples containing ≥ 15 wt% nickel oxide and calcined at ≥ 750°C. Significant changes in texture, surface acidity and catalytic activity were found as a result of the effects of thermal treatment and chemical composition. Incorporation of fluoride ion greatly increased the surface acidity and consequently enhanced the dehydration activity. Dehydration activity is related to the amount of surface acidity while the dehydrogenation of this alcohol is sensitive to NiO content.

Keywords: NiO supported zirconia; acidity of solid catalyst; isopropanol conversion.

1. Introduction

Metal oxides have a wide range of industrial applications including chemical sensors, microelectronic materials, ceramics and catalysis. In heterogeneous catalysis, metal oxides can be used as either active catalysts or supports for dispersing catalytically active metal catalysts [1, 2].

Among various metal oxides, zirconia is of a particular interest and has received widespread attention due to its thermal stability and mechanical properties. Moreover, zirconia is claimed to be a good catalyst that has acidic, basic, reducing and oxidizing surface properties. In modern industry zirconia has been widely used in various fields such as high-temperature fuel cells [3, 4], structural ceramics [5], gas sensors [6, 7], and as an insulator in a metal oxide semiconductor devices [8, 9]. Zirconia was used also as support and / or catalyst material with unique properties in a great variety of reactions. As a support zirconia supported metal and metal oxides have been used in numerous catalytic reactions such as CO oxidation [10, 11], water gas shift reaction [12, 13] and selective hydrogenation of unsaturated organic compounds [14]. While as an active catalyst component it has been used for catalytic reactions like alkene isomerization [15], alcohol dehydration [16] and hydrogenation, dehydrogenation of hydrocarbon [17]. Moreover, ZrO_2 can be used as a promoter to improve the catalytic performance of the catalysts, for example ZrO_2 additive improve the activity and thermal stability of Au/FeO_3 catalyst for low temperature water gas shift reaction [18].

Pure zirconia has three different crystal structures: monoclinic; m-ZrO_2, tetragonal; t-ZrO_2 and cubic; c-ZrO_2 [19]. It is worth noting that the method of preparation and its conditions (temperature, additives and among others) greatly influence the phase structure of the synthesized zirconia and hence significantly influences its physical properties. ZrO_2 when modified with sulfate ions forms a highly acidic catalyst with stabilizing the tetragonal polymorph [20]. The acidic and catalytic properties of sulfated zirconia-based catalysts

depend on a number of preparative parameters, among which particularly important are nature of sulfation procedure, sulfating agent, precipitation procedure [21], thermal treatment, hydration degree and addition of transition metals as promoters [22, 23].

Numerous studies have also been devoted to NiO-based catalysts such as NiO-AlO_3 and NiO-SiO_2 systems which are widely used as catalysts for the oxidative dehydrogenation of ethane to ethylene, NO reduction by CO and CH_4-CO reforming. The surface properties and the catalytic performance of these catalyst systems have been reported [24-26].

The aim of the present work is to investigate the structural properties and thermal stability of ZrO_2 and NiO-ZrO_2 catalysts derived from NaOH-$Na_2C_2O_4$ assisted co-precipitation method. The effects of doping with fluoride ion and calcination temperatures on the structural, textural and acidic properties of ZrO_2 and NiO-ZrO_2 catalysts were also studied. The catalytic performance of the prepared catalysts towards isopropanol conversion was investigated.

2. Experimental

2.1. Catalyst preparation

Pure $Zr(OH)_4$ gel was prepared by a drop-wise addition of $Na_2C_2O_4$-NaOH solution with mole ratio of 1/2 ($Na_2C_2O_4$, 0.5M) to an aqueous solution of $ZrOCl_2 \cdot 8H_2O$. Mixtures of $Zr(OH)_4$ and $Ni(OH)_2$ gels were prepared by co-precipitation from mixed solutions of $ZrOCl_2 \cdot 8H_2O$ and $NiCl_2 \cdot 6H_2O$ with $Na_2C_2O_4$-NaOH solution to contain 5, 10, 15 and 25 wt% NiO respectively. The drop-wise addition of $Na_2C_2O_4$-NaOH solution was continued at 313 K with vigorous stirring until pH = 9. The resulting gels were separated by filtration, washing several times with bidistilled water till free from chloride ions and drying at 373 K for 24 h.

Two fluoride ion doped samples were also obtained by incipient wetness impregnation method. Pure $Zr(OH)_4$ and the sample containing 15 wt% NiO were treated with ammonium

fluoride solutions with fluoride content of 6 wt%. The obtained pastes were dried at 373K for 24h.

All the gels were calcined for 6h at 550°, 650°, 750°, and 850°C respectively. In the designation of the investigated samples, the letters **Z**, **N**, **F** denotes to ZrO_2, NiO and fluoride ion doped samples respectively. The roman numbers **I**, **II**, **III** and **IV** referred to the samples calcined at 550°, 650°, 750°, and 850°C, while the Arabic numbers **5**, **10**, **15** and **25** represents NiO wt% loading. Accordingly therefore the designation **ZN15FII** refers to a ZrO_2-NiO sample containing 15 wt% NiO, doped with fluoride ion and calcined at 650°C.

2.2. Techniques of characterization

2.2.1. Thermal analysis

DTA analysis of various uncalcined samples was carried out using Shimadzu DTA-50 at a heating rate of 10°C min^{-1} in a flow of 30 ml min^{-1} N_2 gas.

2.2.2. X-Ray diffraction (XRD)

X-Ray powder diffraction (XRD) patterns of the calcined samples were recorded using PANalytical, X-Pert PRO diffractometer with nickel filtered Cu K_α radiation over the 2θ range from 2° to 80°. The crystal sizes of the investigated samples were calculated from XRD line broadening using the Scherrer's equation [27]. The characteristic peaks at 2θ = 28.2° and 31.5° for ($\bar{1}$11) and (111) reflexes respectively were assigned to monoclinic phase in ZrO_2, while the peak at 2θ=30.2° for the (111) reflex was assigned to tetragonal phase in ZrO_2.

The percents of tetragonal and monoclinic phases in ZrO_2 were determined by means of their Gaussian areas "*h* x *w*" where *h* and *w* are the height and half-height width of the corresponding XRD characteristic peak using the following relations [28]:

$$\%\ Monoclinic\ phase = \frac{\sum(hxw)_{m-ZrO_2\ phase(M)}}{\sum(hxw)_{m-ZrO_2\ phase(M),\ t-ZrO_2\ phase(T)}}$$

$$\% \, Tetragonal\, phase = \frac{\sum(hxw)_{t-ZrO_2\, phase(T)}}{\sum(hxw)_{m-ZrO_2\, phase(M),\ t-ZrO_2\, phase(T)}}$$

2.2.3. Nitrogen physisorption

Nitrogen adsorption-desorption isotherms were measured at 77 K using Quantachrome, Nova 3200. Samples were degassed under a vacuum of 10^{-3} Torr for 2h at 423 K prior to the adsorption experiments. Specific surface areas were calculated using BET method (S_{BET}) and the existence of microporosity was tested from t-plot constructions.

2.2.4. Surface acidity measurements

The total acidity of the prepared samples was estimated by means of potentiometric n-butyl amine titration method [29]. 0.2 gram of the catalyst was suspended in 20 ml of acetonitrile and stirred for 2 h. The electrode potential variation of the suspended sample with the addition of 0.025 M n-butyl amine was measured using an Orion 420 digital a model with a double junction electrode. The addition continued till no further change of mV recorded.

2.2.5. Catalytic activity measurements

The catalytic conversion of isopropanol was carried out using a pulse microcatalytic system connected to a flame ionization detector (Hewlett Packard 5890A gas chromatograph). Prior to any catalytic run, the catalyst (100 mg) was activated for 30 minutes at the desired reaction temperature. Nitrogen was used as a carrier gas in all catalytic measurements and 1×10^{-3} ml sample of isopropanol was injected on to the catalyst in the form of pulse using a microsuringe.

3. Results and discussion:

3.1. Thermal analysis

The differential thermograms of fluoride ion undoped samples pre-dried at 363 K are shown in (fig.1). Evidently, two endothermic effects are exhibited by all samples. The first

endothermic effects shows its maximum at 95-110°C and was attributed to the removal of physisorbed water. The second endothermic effect takes place at 245°-280°C leading to more developed peaks with their location shifted to higher temperatures with increasing NiO content. This endothermic effect may be related to the dehydroxylation of the two metal hydroxides. In case of NiO-ZrO_2 catalysts, NiO influences the phase transition of ZrO_2. Thus, Z sample (pure $Zr(OH)_4$) exhibited an exothermic effect at 437°C. This effect was exhibited at 485°, 558°, 607° and 650°C for **ZN5**, **ZN10**, **ZN15** and **ZN25** respectively, i.e. the position of the exotherm shifts to higher temperature with the increase in nickel oxide content. Moreover, the area of the peak characterizing this exothermic effect continuously decreases with the increase in NiO content. These exotherms may account for the crystallization of ZrO_2 to metastable tetragonal phase [30]. This new phase (t-ZrO_2) has probably different specific heat compared with hydroxide.

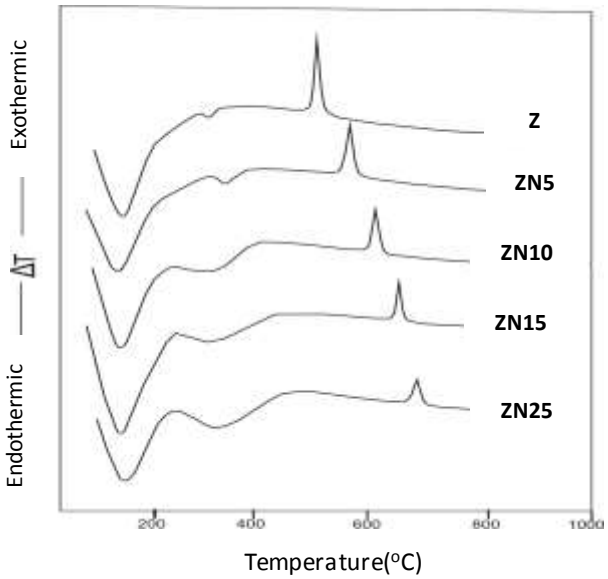

Fig. 1. DTA curves of **Z**, **ZN5**, **ZN10**, **ZN15** and **ZN25** gels.

The differential thermograms of **ZF** and **ZN15F** samples are shown in (fig. 2). Evidently, **ZF** and **ZN15F** samples show an additional endothermic effect at around 400°C which may be attributed to the decomposition of ammonium salt. Moreover, for one and the same chemical composition the area of the exothermic peak characterizing the crystallization of ZrO_2 decreases due to the addition of fluoride ion.

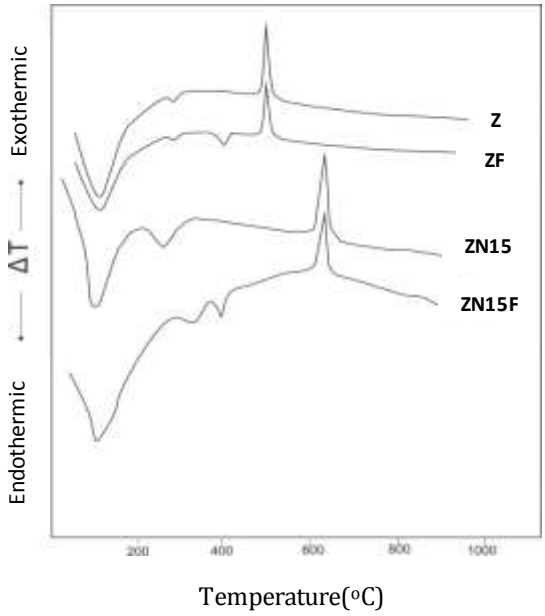

Fig. 2. DTA curves of **Z, ZF**, **ZN15** and **ZN15F** gels.

3.2. Crystal structure

The XRD patterns of NiO-ZrO_2 samples calcined at 550°C and those for **Z** and **ZN15** samples calcined at different temperatures are illustrated in (figs. 3-5). The corresponding phase compositions are presented in Tables 1 and 2. As seen from (figs. 3-5) the chemical composition and the calcination temperature show significant impact on both crystal phase and crystallite size. The degree of crystallinity of tetragonal phase decreases gradually by increasing NiO content up to 25 wt% (fig. 3). It seems that the increase of NiO content to a certain limit is accompanied by crystallite growth and to instability of tetragonal phase. Most published studies agree that incorporation of some additive materials retards crystallization of zirconia support and enhances its amorphous structure [31, 32]. In fact, the tetragonal phase

should be formed above 1170°C, but in many cases zirconia obtained by precipitation from aqueous salt solution can be occurred as metastable tetragonal phase at lower temperature [33]. Moreover, the transformation of the metastable tetragonal into the monoclinic phase was probably due to the lower surface energy of the tetragonal phase compared to monoclinic phase [34, 35]. Figure 3 reveals also the absence of diffraction lines characteristics of NiO phase for all NiO-ZrO_2 samples calcined at 550°C. This may be attributed to the high surface area of zirconia support which allowed the high dispersion of NiO species and inhibited the formation of NiO crystallites.

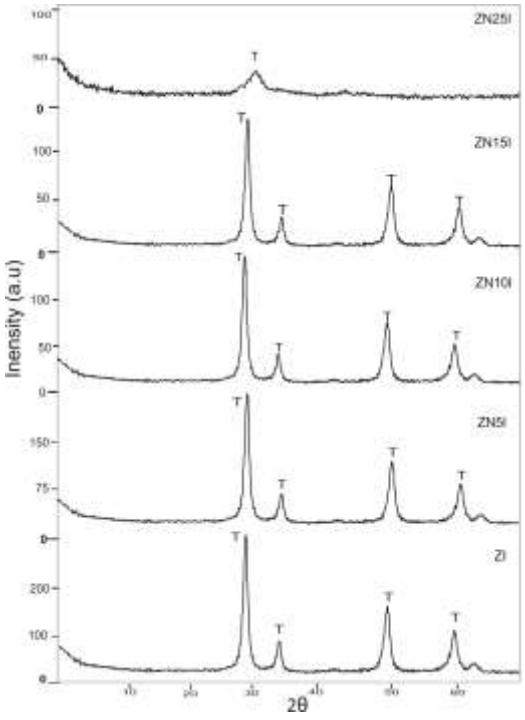

Fig. 3. XRD patterns of ZrO_2 and NiO-ZrO_2 samples calcined at 550°C.

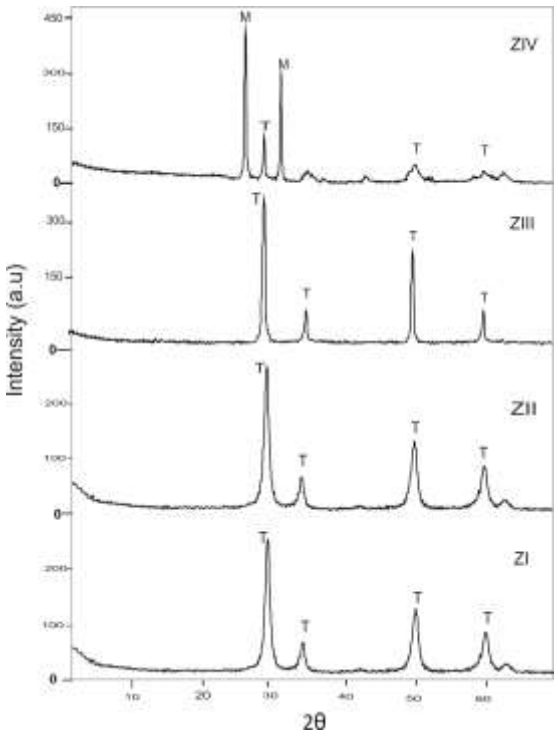

Fig. 4. XRD patterns of ZrO_2 sample calcined at different temperatures.

The XRD patterns of **Z** and **ZN15** samples calcined at different temperatures exhibited in some cases biphasic mixture of tetragonal and monoclinic phase as indicated from figures (4, 5). It is interesting to note from (fig. 5) that the tetragonal phase transformation to monoclinic one started at 750° and increases with the increase of calcination temperature from 750° to 850°C. In agreement with DTA results, the increase of the calcination temperature leads to crystallite growth due to loss of water content which leads to instability of tetragonal

phase and then the transition from the tetragonal phase to the monoclinic phase occurs [36, 37]. Figure 5 indicates also that the absence of NiO diffraction lines for **ZN15** sample calcined at $\leq 650^{o}$C. This may be due to the high dispersion of NiO species and / or to its amorphous nature. Very weak reflection lines at $2\theta = 43.5^{o}, 47^{o}$ and 60^{o} appear after calcination at $\geq 750^{o}$C corresponding respectively to the planes of (III),(I02)and (200) which can be assigned to the presence of traces amount of cubic NiO.

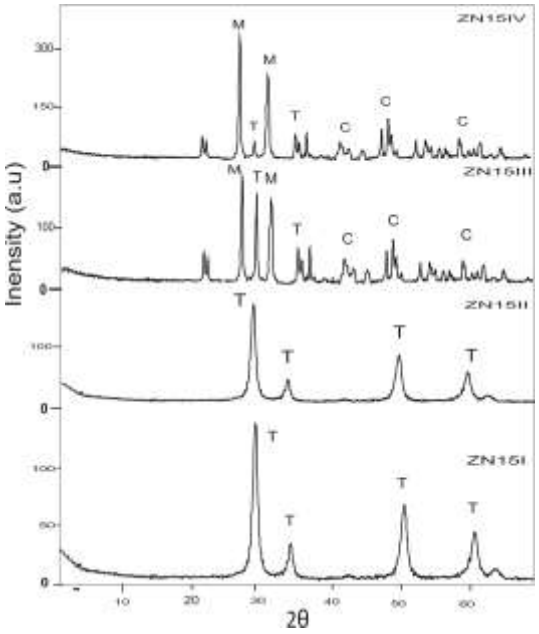

Fig. 5. XRD patterns of **ZN15** sample calcined at different temperatures.

The XRD patterns of fluoride ion doped samples were also determined (not illustrated) and their results obtained are summarized in Table 2. It can be seen from Tables 1 and 2 that fluoride ion doped samples measure slightly lower values of crystallite size and degree of crystallinity than undoped samples. Moreover, fluorinated samples show XRD patterns more or less simillar to those of undoped **Z** and **ZN15** samples. This means that addition of fluoride ion dopant to **Z** and **ZN15** samples slightly affected their structural characteristics.

Table 1. Crystal structure and crystal size of undoped catalysts.

Catalyst	Phases detected*	% Major phase	Crystal size (D) of major phase (nm)	Degree of crystallinity (a.u)**		E_s (kJ mole^{-1})
				T(2θ=30.3)	M(2θ=28.2)	
ZI	T	100(T)	29.5	225	_	13.8
ZII	T	100(T)	38.0	268	_	
ZIII	T	100 (T)	44.5	380	_	
ZIV	M+T	83.8(M)	49.5	130	300	
ZN5I	T	100(T)	19.5	210	_	
ZN10I	T	100(T)	23.4	190	_	
ZN15I	T	100(T)	29.5	145	_	
ZN25I	T	100(T)	39.5	36	_	
ZN15I	T	100(T)	29.5	145	_	24.89
ZN15II	T	100(T)	21.4	282	_	
ZN15III	M+T+C	64.1(M)	31.0	178	195	
ZN15IV	M+T+C	91.3(M)	40.5	48	343	

* M: monoclinic ZrO_2, T: tetragonal ZrO_2 and C: cubic NiO.

** The peak height of the major line of each phase was taken as measure for the degree of crystallinity of the ZrO_2.

Finally, it is worth noting that for one and the same chemical composition the degree of crystallinity was found to increase with the increase of calcination temperature, while for the samples calcined at 550°C the degree of crystallinity decreases gradually with the increase of NiO content.

Table 2. Crystal structure and crystal size of the samples doped with fluoride ion.

Catalyst	Phases detected*	% Major phase	Crystal size (D)of major phase (nm)	Degree of crystallinity (a.u)**		E_s (k J mole^{-1})
				T(2θ=30.3)	M(2θ=28.2)	
ZFI	T	100 (T)	30.0	280	_	13.21
ZFII	T	100 (T)	36.8	265	_	
ZFIII	T	100 (T)	42.0	290	_	
ZFIV	M+T	86.2(M)	48.5	110	210	
ZN15FI	T	100 (T)	18.0	130	_	23.16
ZN15FII	T	100 (T)	22.0	212	_	
ZN15FIII	M+T+C	73.6(M)	30.0	140	118	
ZN15FIV	M+T+C	85.5(M)	41.0	24	160	

* M: monoclinic ZrO_2, T: tetragonal ZrO_2 and C: cubic NiO.

** The peak height of the major line of each phase was taken as a measure for the degree of crystallinity of ZrO_2.

3.3. Textural properties

All the samples investigated showed more or less similar nitrogen adsorption isotherms. Although some minor changes are there, yet all the isotherms belong to type IV according to IUPAC [38], indicating thus the predominance of the mesopore structure for all the samples. Representative adsorption-desorption isotherms are illustrated in (fig.6). The textural parameters include specific surface area (S_{BET}, m^2g^{-1}) and total pore volume (V_p, ml g^{-1}) were determined from the analysis of these isotherms. The main pore radius $\bar{r}$(Å) was calculated from the relationship: $\bar{r}(Å) = (2V_p \times 10^4) / S_{BET}$. The textural parameters (S_{BET}, V_p and $\bar{r}$ are listed in columns (2, 4 and 5) of Table 3.

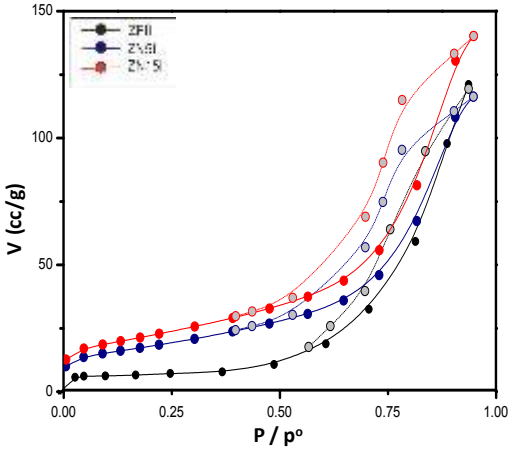

Fig. 6. Nitrogen adsorption-desorption isotherms of some selected samples.

The V_l-t method suggested by de Boer was also employed to calculate the surface area, S_t (m^2g^{-1}) from the slope of linear part of the V_l-t plots which passes through the origin [39]. The calculated S_t areas are compared with S_{BET} areas in columns 3 and 2 Table 3, respectively. The V_l-t plots of all samples investigated (not illustrated) showed an upward deviation indicating the domination of the mesopore structure for all the samples investigated. This conclusion is also supported from comparing the values of $\bar{r}$ given in Table 3 which shows that the $\bar{r}$ values of all samples vary between 30-96 Å.

Inspection of the textural data in columns (2-5) of Table 3 reveals the following:

1. The values of S_{BET} and S_t for all samples investigated are close to each other which justify the correct choice of standard t curve used in pore analysis.
2. For the samples calcined at 550°C the surface area increases gradually upon increasing NiO content, reaching a maximum at 15 wt% NiO. Further increase of NiO content beyond 15wt% was associated with a significant decrease in both the surface area and the total pore volume. At low NiO content up to 15 wt%, two phenomena in principle could be acting. One is interconnection between original ZrO_2 grains with the incorporated NiO particles, while the other is simultaneous filling of ZrO_2 pores. With

thermal treatment the two effects may lead to the creation of new mesopores as well as enhancing the disaggregation of the resulting particles. These effects could explain the increase of the surface area as observed in Table 3. At higher NiO content the large species of NiO particles present start to block some of the pores of the catalyst, thereby reducing surface and the total pore volume.

3. Finally, for one and the same chemical composition the surface area and the total pore volume decreased with increasing the calcination temperature from 550º to 850ºC. The increase of the calcination temperature leads to crystallite growth due to the elimination of water content. This process led to the instability of tetragonal phase indicating the sintering of zirconia particles which led to decrease both S_{BET} area and total pore volume. Fluoride ion undoped samples exhibit slightly higher values of surface parameters than doped one.

It is interesting to show how the crystallite size of initial grains of zirconia is affected by the thermal treatment, where the grains' growth of the prepared particles takes place. After crystallization the particles continue to increase in size with increasing calcination temperature through the process of sintering as supported by the increased intensity of the XRD diffraction lines. The variation of the crystallite size (D) of t-ZrO_2 phase as calculated from its XRD line proading with the preheated temperature, T, (550º-850ºC) permit the calculation of activation energy of sintering (E_s) of t-ZrO_2 phase using Arrhenius equation:

$$D = A\, e^{-E_s/RT}$$

Where A is the frequency factor of Arrhenius equation and E_s is the activation energy of sintering process of such sample [40]. By plotting Ln D versus 1/T, a straight line is obtained whose slope and intercept permit the calculation of E_s and A. The Arrhenius plots for undoped and fluoride ion doped **Z** and **ZN15** samples are shown in (fig.7). The calculated E_s values are 13.8 and 24.9 kJ mole^{-1} for **Z** and **ZN15** samples. These results suggested that pure

zirconia is respond to sintering faster than NiO supported samples. One can concluded that incorporation of NiO into ZrO_2 support led to improve its thermal stability. The obtained E_s values of the two samples after doping with fluoride ion were found to be 13.21 and 23.16 kJ $mole^{-1}$. It seems that addition of fluoride ion slightly decreased the thermal stability of the two samples. These results complement also the results obtained from XRD data and confirm the increase of calcination temperature and consequently the increase of crystallite size was the reason for the pronounced decrease in BET surface area of the calcined samples.

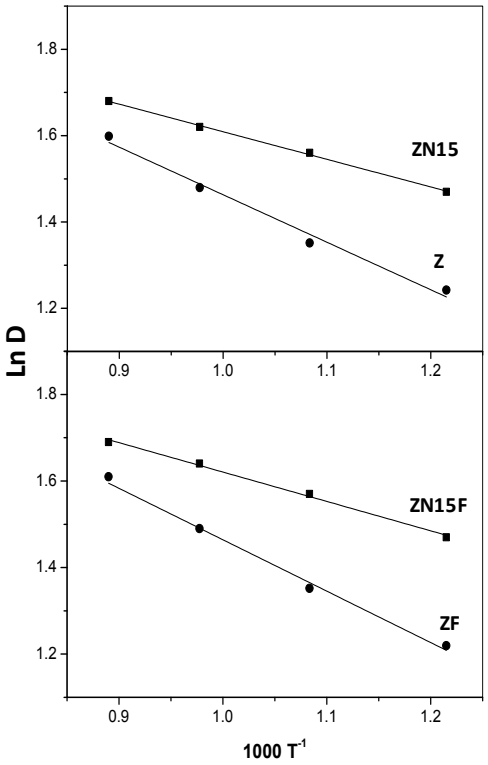

Fig. 7. Arrhenius plots of activation energy of sintering for tested samples.

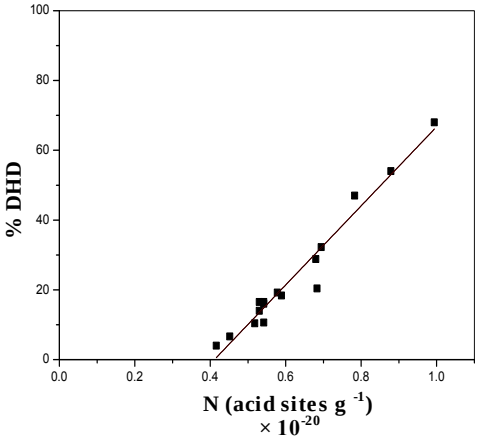

Fig. 8. DHD of isopropanol as a function of acid sites per gram for **ZI** sample.

3.4. Surface acidity

As a criterion to interpret the obtained results, it has been reported that the initial electrode potential (E_i), indicates the maximum acid strength of the acid sites, and the value of ml $_{eq.amine}$ per gram solid where the plateau of titration curve is reached indicates the total acidity [41]. Moreover, the acid strength of these sites can be classified according to the

following scale: (E_i > 100 mV) very strong sites, (0 mV< E_i < 100 mV) strong sites, (-100 mV < E_i < 0 mV) weak sites and (E_i < -100 mV) very weak sites [42]. The values of E_i and the total number of acid sites per gram catalyst are listed in columns 6 and 7of Table 3. Generally the total acidity expressed as a number of acid sites per gram catalyst, N (acid sites g^{-1}) continuously decreases with rise of calcination temperature. Probably the rise of calcination temperature partially removes a fraction of surface acid sites. This was the case for all the catalysts under investigation. It is also evident that the number of acid sites per gram continuously decreases with the increase in NiO content. On contrary the acid strength as indicated from the E_i values was found to increase with the increase in NiO content. This may be taken as evidence that NiO removes weak acid sites and concentrate strong one. Finally **ZFI** sample shows the highest acid amount among the other samples while **ZN15IV** shows the lowest one.

3.5. Conversion of isopropanol

Conversion of isopropanol proceeds through two main reaction paths namely dehydration (DHD) to propene and dehydrogenation (DHG) to acetone. DHD proceeds on acid sites [43], while DHG is related to the P-type conductivity and the electronic characteristics of the solid catalyst [44]. The percent DHD and DHG activities at 573K and at flow rate of the Nitrogen carrier gas of 25 ml min^{-1} are listed in columns (8 and 9) of Table 3.

Table 3. Surface characteristics, acidic and catalytic properties of the investigated catalysts.

Sample	S_{BET} (m^2g^{-1})	S_t (m^2g^{-1})	V_p (ml g^{-1})	$\bar{r}$ (Å)	E_i mV	N(acid sites g^{-1}) $\times 10^{-20}$	% DHD	% DHG
ZI	76.03	70.5	0.21	54.4	41	0.72	37.3	0
ZII	58.0	58.2	0.18	56.7	35	0.680	28.8	0
ZIII	50.6	28.4	0.13	72.2	30	0.590	18.4	0
ZIV	18	11.8	0.09	96.0	13	0.518	10.4	0
ZN5I	98.6	100.2	0.34	96.08	52	0.578	20.4	14.6
ZN10I	127.6	130.4	0.38	71.37	62	0.530	19.2	20.4
ZN15I	138.0	144.0	0.342	53.46	70	0.542	16.5	28.6
ZN25I	100.0	98.0	0.159	31.0	78	0.430	10.6	38.0
ZN15I	138.0	144.0	0.342	53.46	70	0.542	16.5	28.6
ZN15II	80.0	78.6	0.26	59.8	71	0.542	16.0	27.8
ZN15III	36.0	34.4	0.18	68.53	56	0.452	6.6	9.6
ZN15IV	20.4	18.0	0.114	72.0	44	0.380	4.0	6.0
ZFI	70.6	69.5	0.206	58.3	81	0.994	68.0	0
ZFII	50.4	49.0	0.189	75.0	72	0.78	47.0	0
ZFIII	27.8	31.0	0.14	90.3	63	0.693	32.3	0
ZFIV	12.4	20.4	0.102	113	66	0.530	14.0	0
ZN15FI	118.0	117.6	0.306	51.8	98	0.879	54.0	12.0

The data in this table indicates that: (i) NiO-ZrO_2 catalysts measure DHD and DHG activities while ZrO_2 catalysts shows only DHD activities. (ii) In general, the DHD activities decreased while the DHG activities increased with increasing NiO content. (iii) The DHD activities of **ZI** samples markedly increase with fluoride ion doping. The observed increase in the DHD activity of pure ZrO_2 sample due to doping with fluoride ion reflected an effective

increase in the concentration of the surface acid sites which represent the catalytically active sites for the dehydration of alcohols.(iv) Finally for one and the same chemical composition (i.e. for **ZN15** sample) the DHD and DHG activities remain approximately constant with increase in calcination temperature from 550°C to 650°C and then decrease with further increase up to 850°C. This finding may be attributed to restriction of catalytic active constitutes due to partially removes a fraction of surface acidities, increasing of degree of crystallinity of detected phases and or sintering process.

No relation was found between either the DHD or DHG activities on the one hand and the total S_{BET} areas on the other hand. The results reveal also that DHD activity is not sensitive to the strength of the acid sites. This indicated by significant DHD activity of **ZI** sample which has a low value of acid strength (E_i= 41mV). Moreover, NiO-ZrO_2 samples measure lower values of DHD activity although they have relatively higher values of acid strength (E_i=44-78mV) in comparing with that of pure ZrO_2. Evidently dehydration of this alcohol was found related to the number of acid sites per gram where a good straight line was obtained between % DHD activity and N (acid sites g^{-1}) (fig.8). Extension of the straight line in (fig.8) intersects the N (acid sites) axis indicating that a minimum number of acid sites per gram catalyst are necessary to initiate dehydration of isopropanol. It seems that dehydration of isopropanol is related to the number of acid sites on the surface of the catalyst rather than to the strength of these acid sites, agrees well with previous studies [45, 46].

4. Conclusions

Stabilization of the t-ZrO_2 phase was maintained upon calcination up to ≤ 750°C. Thermal treatment at > 750°C resulted in phase transformation from tetragonal to monoclinic zirconia due to the increase of crystallite size above the critical size of tetragonal phase. The addition of NiO to ZrO_2 influences the phase transition of ZrO_2. No spinel structure was detected by both DTA and XRD techniques and only traces of c-NiO was detected for

samples containing ≥ 15 wt% NiO calcined at ≥ 750°C. The crystallite size of initial grains of ZrO_2 is affected by the thermal treatment where the size of the crystal increases with increase in calcination temperature due to sintering process. The results agree well with those obtained from XRD data and confirm that the increase in the crystallite size was the reason for the pronounced decrease in BET surface area upon increasing thermal temperature. Fluoride ion doping slightly affected the structure and texture properties of doped samples but rather markedly increased the concentration of surface acidity which represent the catalytically active constituents taking part in the DHD of alcohol. Pure and fluoride ion doped zirconia catalysts exhibit no DHG activity, whereas supported with NiO favored the conversion of isopropanol to propene and acetone. DHD to propene is related to the number of acid sites per unit weight while DHG to acetone is sensitive to NiO content.

References

[1] CHEN M.S., GOODMAN D.W., *J. Phys.: Condens. Matter*., 20 (2008), 4013.

[2] SHAIKHTDMOV S., FREUND H., *Annu. Rev. Phys. Chem.*, 63 (2012), 619.

[3] JACOBSON A., *Chem. Mater.*, 22 (2010), 660.

[4] LAGUNA-BERCERO M.A., *J. Power Sources*, 203 (2012), 4.

[5] AKBAR S., DUTTA P., LEE C.H., *Appl. Ceram. Technol.*, 3 (2006), 302.

[6] FERGUS J.W., *Sensor. Actuat. B-Chem.*, 121(2007), 652.

[7] KOROTECENKOV G., DOHAN S., STETTER J.R., *Chem. Rev.*, 109 (2009), 1402.

[8] STEMMER S., J.*Vac. Sci. Technol. B* , 22 (2004), 791.

[9] CHIANG C.K., WU C.H., LIU C.C., LIN J.F., YANG C.L., WU J.W., WANG S.J., *Jpn. J. Appl. Phys.*, (2012), 51.

[10] ZHANG X., SHI H., XU B.Q., *Catal. Today*, 122 (2007), 330.

[11] COMOTTI M., LI W.C., SPLIETHOFF B., SCHUTH F., *J.Am. Chem. Soc.*, 128 (3) (2006), 917.

[12] IDAKIEV V., TABAKOVA T., NAYDENOV A.Z., YUAN Y., SU B.L., *Appl. Catal. B*-Environ., 63 (2006), 178.

[13] LI J., TA N., SONG W., ZHAN E.S., SHEN W.J., *Gold Bull.*, 42 (2009), 48.

[14] ZHANG X., SHI H., XU B.Q., *Angew. Chem. Int. Edit.*, 44 (2005), 7132.

[15] NAKANO Y., IIZUKA T., HATTORI H., TANABE T., *J. Catal.*, 57 (1979), 1.

[16] FERINO I., CASULA M.F., CORRIAS A., CUTRUFELLO M.G., MONACI R., PASCHINA G., *Phys. Chem. Chem. Phys.*, 2 (2000), 1847.

[17] TANABE K., YAMAGUCHI T., *Catal. Today*, 20 (1994), 185.

[18] ZHANG F., ZHENG Q., WEI K., LIN X., ZHANG H., LI J., CAO Y., *Catal. Lett.*, 108 (2006), 131.

[19] MUNOZ M. C., GALLEGO S., BELTRAN J.I., CERDA J., *Surf. Sci. Rep.*, 61 (2006), 303.

[20] BENITEZ J.J., ALVERO R., CARRIZOSA I., ODRIOZOLA J.A., *Catal. Today*, 9 **(**1991**),** 53.

[21] COMELLI R.A., VERA C.R., PAVERA J.M., *J. Catal.*, 151 **(**1995), 96.

[22] YADAV G.D., MURKUTE A.D., *J. Catal.*, 24 (2004), 218.

[23] BOLIS V., MAGNACCA G., CERRATO G., MORTERRA C., *Top. Catal.*, 19 **(**2002), 259.

[24] ZHANG X., LIU J., JING Y., XIE Y., *Appl. Catal. A-Gen.*, 240 (2003) ,143.

[25] ANGELIDIS T.N., PAPAPETROU M., *Stud. Surf. Sci. Catal.*, 133 (2001), 131.

[26] CHEN X., HONDA K., ZHANG Z., *Appl. Catal. A-Gen.*, 288 (2005), 86.

[27] CULLITY B.D., *Elements of X-Ray Diffraction*, Addison-Wesley, California, 1978.

[28] SU C., LI J., HE D., CHENG Z., ZHU Q., *Appl. Catal. A-Gen*., 202 (2000), 81.

[29] RAO K.N., REDDY K.M., LINGAISH N., SURYANARAYANA I., PRASAD P.S., *Appl. Catal. A-Gen*., 300 (2006), 139.

[30] LI G., LI W., ZHANG M., TAO K., *Catal. Today***,** 93-95 (2004), 595.

[31] AHMED A.I., EL HAKAM S.A., SAMRA S.E., E-KHOLY A.A., KHDER A.S., *Colloid. Surface* A., 317 **(**2008), 62.

[32] SOHN J.R., PARK W.C., *Appl. Catal. A-Gen*., 230 (2002), 11.

[33] FARCASIU D.,LI J.Q., CAMERON S., *Appl. Catal. A-Gen*., 154 (1997), 173.

[34] TANI E., YOSHIMURA M., SOMIYA S., *J. Am. Ceram. Soc.*, 66 (1983), 11.

[35] OSENDI M.I., MOYA J., SERNA C.J., SORIA J., *J. Am. Ceram. Soc.*, 68 (1985), 135.

[36] YAMAGUCHI T., TANABE T., *Mater. Chem. Phys.*, 16 (1987), 67.

[37] SRINIVASON R., KEOG R A., MILBURN D R., DAVIS B.H., *J. Catal.*, 153 (1995), 123.

[38] XU R.R., BANG W.Q., *Chemistry of molecule sieves and mesoporous materials*, Science Press, Beijing, 2004, p.173.

[39] DE BOER J.H., *The structure and preperties of porous materials*, Butterworth, London, 1958.

[40] MOKHTAR M., BASAHL S.N., ALI T.T., *J. Mater. Sci.*, 48 (2013), 2705.

[41] PIZZIO L., VAZQUEZ P.G., CACERES C.V., BLANCO M.N., *Catal. Lett.*, 93 **(**2004) 67.

[42] PIZZIO L., BLANCO M.N., *Appl. Catal. A-Gen.*, 255 **(**2003), 265.

[43] MOSTAFA M.R.,YOUSSEF A.M., *Mater. Lett.*, 34 (1998), 405.

[44] PEPE F., ANGELETTI C., ROSSI S.D., *J. Catal.*, 118 (1989), 1.

[45] MOSTAFA M.R., YOUSSEF A.M., HASSAN S.M., *Mater. Lett.*, 12 (1991), 207.

[46] MOSTAFA M.R., *AFINIDAD*, 51 (1994), 445.

Table 1.Crystal structure and crystal size of undoped catalysts.

Catalyst	Phases detected*	% Major phase	Crystal size (D) of major phase (nm)	Degree of crystallinity (a.u)**		E_s (kJ $mole^{-1}$)
				T(2Θ=30.3)	M(2Θ=28.2)	
ZI	T	100(T)	29.5	225	_	13.8
ZII	T	100(T)	38.0	268	_	
ZIII	T	100 (T)	44.5	380	_	
ZIV	M+T	83.8(M)	49.5	130	300	
ZN5I	T	100(T)	19.5	210	_	
ZN10I	T	100(T)	23.4	190	_	
ZN15I	T	100(T)	29.5	145	_	
ZN25I	T	100(T)	39.5	36	_	
ZN15I	T	100(T)	29.5	145	_	24.89
ZN15II	T	100(T)	21.4	282	_	
ZN15III	M+T+C	64.1(M)	31.0	178	195	
ZN15IV	M+T+C	91.3(M)	40.5	48	343	

*M: monoclinic ZrO_2,T : tetragonal ZrO_2 and C: cubic NiO.

**The peak height of the major line of each phase was taken as measure for the degree of crystallinity of the ZrO_2.

Table 2.Crystal structure and crystal size of the samples doped with fluoride ion.

Catalyst	Phases detected*	% Major phase	Crystal size (D)of major phase (nm)	Degree of crystallinity (a.u)**		E_s (k J $mole^{-1}$)
				T(2Θ=30.3)	M(2Θ=28.2)	
ZFI	T	100 (T)	30.0	280	_	13.21
ZFII	T	100 (T)	36.8	265	_	
ZFIII	T	100 (T)	42.0	290	_	
ZFIV	M+T	86.2(M)	48.5	110	210	
ZN15FI	T	100 (T)	18.0	130	_	23.16
ZN15FII	T	100 (T)	22.0	212	_	
ZN15FIII	M+T+C	73.6(M)	30.0	140	118	
ZN15FIV	M+T+C	85.5(M)	41.0	24	160	

*M: monoclinic ZrO_2, T: tetragonal ZrO_2 and C: cubic NiO.

** The peak height of the major line of each phase was taken as a measure for the degree of crystallinity of ZrO_2.

Table 3. Surface characteristics, acidic and catalytic properties of the investigated catalysts.

Sample	S_{BET} (m^2g^{-1})	S_t (m^2g^{-1})	V_p (ml g^{-1})	$\bar{r}$ (Å)	E_i mV	N(acid sites g^{-1}) $\times 10^{-20}$	% DHD	% DHG
ZI	76.03	70.5	0.21	54.4	41	0.72	37.3	0
ZII	58.0	58.2	0.18	56.7	35	0.680	28.8	0
ZIII	50.6	28.4	0.13	72.2	30	0.590	18.4	0
ZIV	18	11.8	0.09	96.0	13	0.518	10.4	0
ZN5I	98.6	100.2	0.34	96.08	52	0.578	20.4	14.6
ZN10I	127.6	130.4	0.38	71.37	62	0.530	19.2	20.4
ZN15I	138.0	144.0	0.342	53.46	70	0.542	16.5	28.6
ZN25I	100.0	98.0	0.159	31.0	78	0.430	10.6	38.0
ZN15I	138.0	144.0	0.342	53.46	70	0.542	16.5	28.6
ZN15II	80.0	78.6	0.26	59.8	71	0.542	16.0	27.8
ZN15III	36.0	34.4	0.18	68.53	56	0.452	6.6	9.6
ZN15IV	20.4	18.0	0.114	72.0	44	0.380	4.0	6.0
ZFI	70.6	69.5	0.206	58.3	81	0.994	68.0	0
ZFII	50.4	49.0	0.189	75.0	72	0.78	47.0	0
ZFIII	27.8	31.0	0.14	90.3	63	0.693	32.3	0
ZFIV	12.4	20.4	0.102	113	66	0.530	14.0	0
ZN15FI	118.0	117.6	0.306	51.8	98	0.879	54.0	12.0

Figure Captions

Figure 1. DTA curves of **Z**, **ZN5**, **ZN10**, **ZN15** and **ZN25** gels.

Figure 2. DTA curves of **Z**, **ZF**, **ZN15** and **ZN15F** gels.

Figure 3. XRD patterns of ZrO_2 and NiO-ZrO_2 samples calcined at 550°C.

Figure 4. XRD patterns of ZrO_2 sample calcined at different temperatures.

Figure 5. XRD patterns of **ZN15** sample calcined at different temperatures.

Figure 6. Nitrogen adsorption-desorption isotherms of some selected samples.

Figure 7. Arrhenius plots of activation energy of sintering for tested samples.

Figure 8. DHD of isopropanol as a function of acid sites per gram for **ZI** sample.

Table 2

Download source file (13.42 MB)

FIGURES

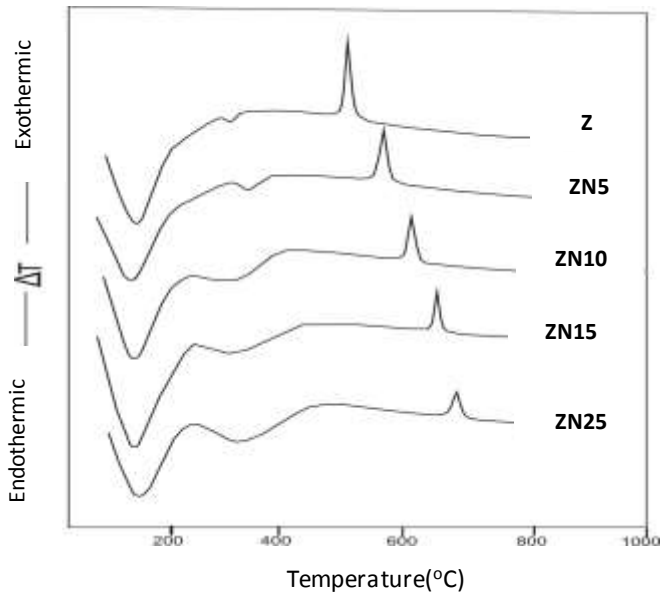

Figure 1

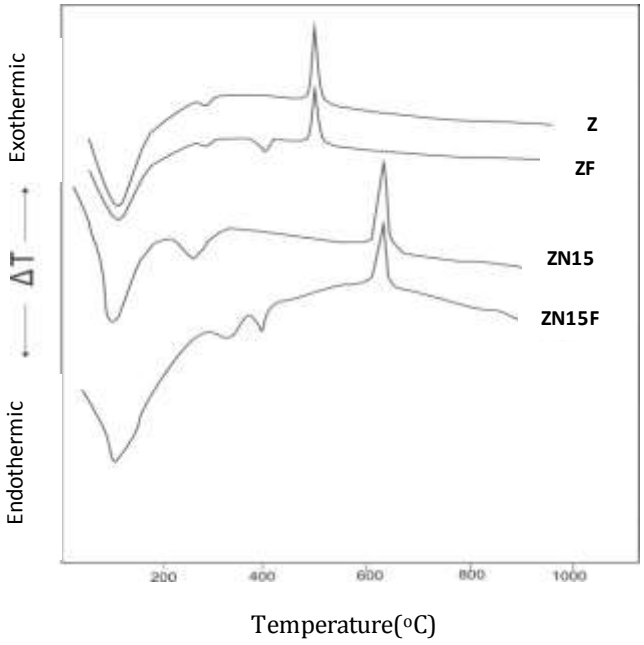

Figure 2

Table 2

Download source file (1

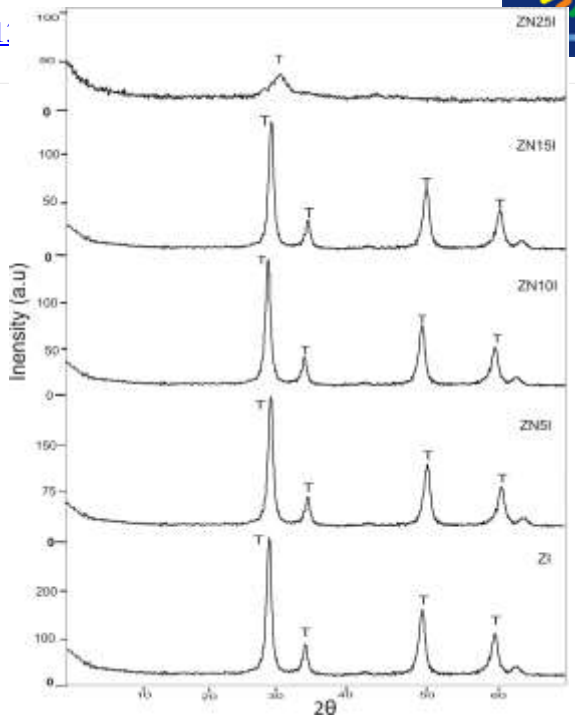

Figure 3

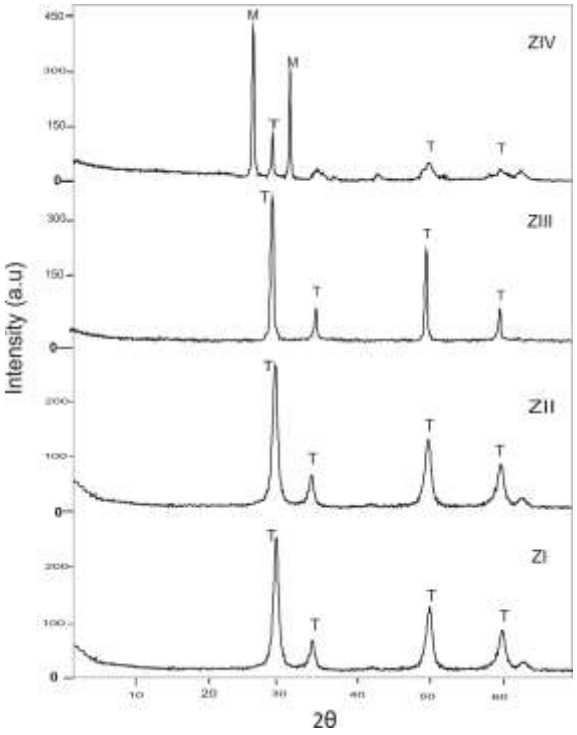

Figure 4

Table 2

Download source file (13.42 MB)

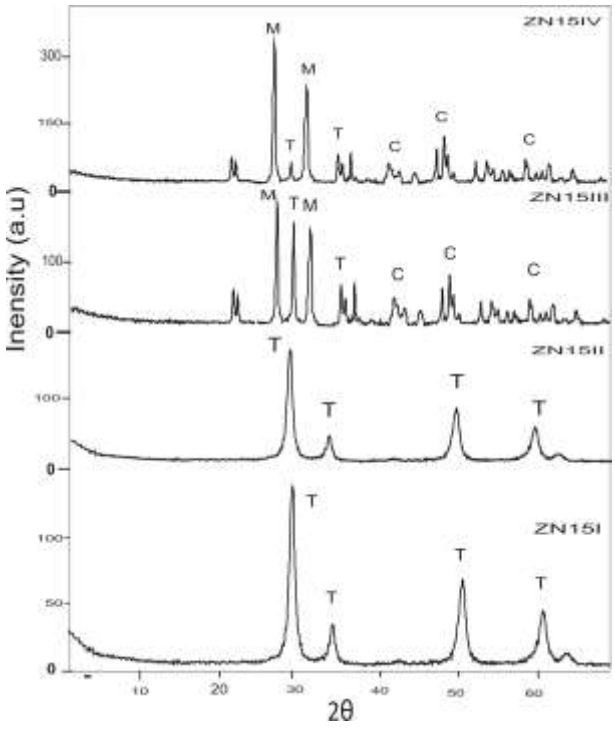

Figure 5

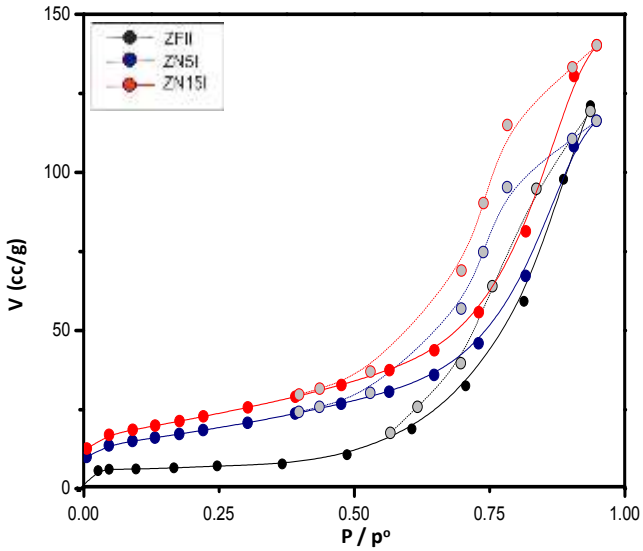

Figure 6

Table 2

Download source file (13.42 MB)

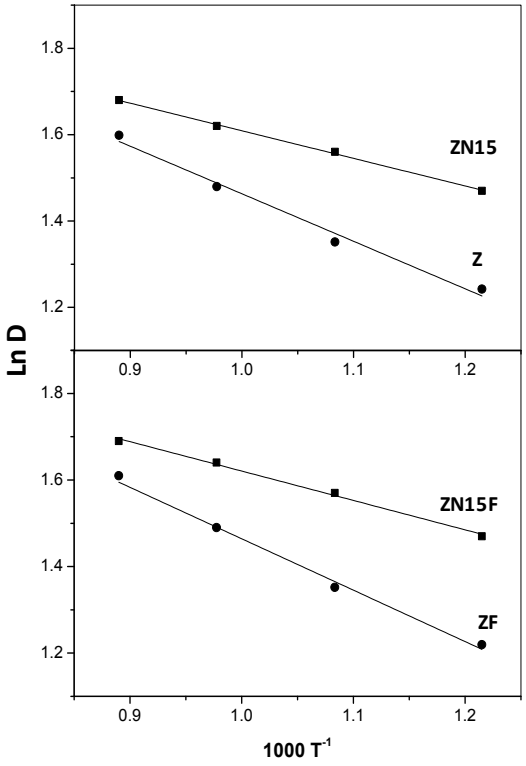

Figure 7

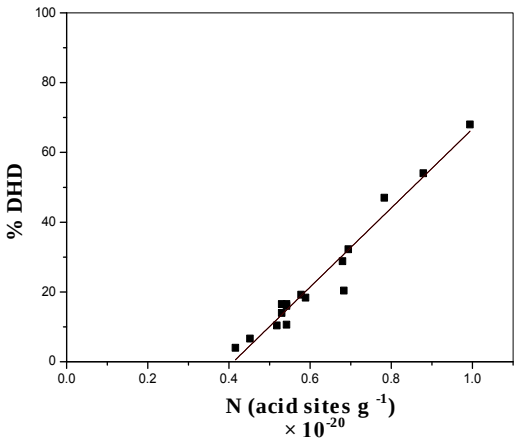

Figure 8

Manuscript body

Manuscript body 1 - Download source file (13.48 MB)

Tables

Table 1 - Download source file (24.19 kB)

Table 2 - Download source file (13.42 MB)